

# The Radio Continuum of the Metal-Deficient Blue Compact Dwarf Galaxy SBS 0335–052

Leslie K. Hunt<sup>1</sup>, Kristy K. Dyer<sup>2,3</sup>, Trinh X. Thuan<sup>4</sup>, and James S. Ulvestad<sup>2</sup>

## ABSTRACT

We present new Very Large Array observations at five frequencies, from 1.4 to 22 GHz, of the extremely low-metallicity blue compact dwarf SBS 0335–052. The radio spectrum shows considerable absorption at 1.49 GHz, and a composite thermal+non-thermal slope. After fitting the data with a variety of models, we find the best-fitting geometry to be one with free-free absorption homogeneously intermixed with the emission of both thermal and non-thermal components. The best-fitting model gives an emission measure  $EM \sim 8 \times 10^7 \text{ pc cm}^{-6}$  and a diameter of the radio-emitting region  $D \approx 17 \text{ pc}$ . The inferred density is  $n_e \sim 2000 \text{ cm}^{-3}$ . The thermal emission comes from an ensemble of  $\sim 9000$  O7 stars, with a massive star-formation rate ( $\geq 5 M_\odot$ ) of  $0.13\text{--}0.15 \text{ yr}^{-1}$ , and a supernova rate of  $0.006 \text{ yr}^{-1}$ . We find evidence for ionized gas emission from stellar winds, since the observed Br $\alpha$  line flux significantly exceeds that inferred from the thermal radio emission. The non-thermal fraction at 5 GHz is  $\sim 0.7$ , corresponding to a non-thermal luminosity of  $\sim 2 \times 10^{20} \text{ W Hz}^{-1}$ . We derive an equipartition magnetic field of  $\sim 0.6\text{--}1 \text{ mG}$ , and a pressure of  $\sim 3 \times 10^{-8} - 1 \times 10^{-7} \text{ dyne cm}^{-2}$ . Because of the young age and compact size of the starburst, it is difficult to interpret the non-thermal radio emission as resulting from diffusion of supernova (SN) accelerated electrons over  $10^7 - 10^8 \text{ yr}$  timescales. Rather, we attribute the non-thermal radio emission to an ensemble of compact SN remnants expanding in a dense interstellar medium. If the radio properties of SBS 0335–052 are representative of star formation in extremely low-metallicity environments, derivations of the star formation rate from the radio continuum in high redshift primordial galaxies need to be reconsidered. Moreover, photometric redshifts inferred from “standard” spectral energy distributions could be incorrect.

---

<sup>1</sup>INAF-Istituto di Radioastronomia-Sez. Firenze, L.go Fermi 5, I-50125 Firenze, Italy; hunt@arcetri.astro.it.

<sup>2</sup>National Radio Astronomy Observatory, P.O. Box O, Socorro, NM 87801, USA: kdye@aoc.nrao.edu, julvesta@cv3.cv.nrao.edu

<sup>3</sup>National Science Foundation Astronomy and Astrophysics Postdoctoral Fellow

<sup>4</sup>Astronomy Department, University of Virginia, Charlottesville, VA 22903, USA: txt@virginia.edu

*Subject headings:* Galaxies: individual: SBS 0335-052; Galaxies: compact; Galaxies: starburst; ISM: supernova remnants; Radio continuum: galaxies

## 1. Introduction

When and how the first episodes of star formation took place remains one of the main questions of modern cosmology. Much effort has been devoted to measuring the cosmic star formation rate (SFR) of the universe as a function of redshift or look-back time initially at ultraviolet wavelengths (e.g., Madau et al. 1996), and more recently in the millimeter and radio regimes (e.g., Blain et al. 1999; Haarsma et al. 2000). Unlike ultraviolet or optical wavelengths, radio emission at  $\gtrsim 1$  GHz is unaffected by dust, which eliminates the need for uncertain extinction corrections. Nevertheless, the conversion of radio luminosity to SFR depends on canonical scaling relations (e.g., Condon 1992) which may not apply to star formation at high redshift.

Primordial star formation occurs in chemically unenriched environments. Besides the high-redshift Ly $\alpha$  absorption systems which are very difficult to study, the only examples we have of such environments are nearby metal-poor galaxies actively forming stars, such as the class of galaxies known as Blue Compact Dwarfs (BCDs). Unlike solar-metallicity star-forming regions, the radio emission in these objects tends to be predominantly thermal rather than non-thermal (Klein, Wielebinski, & Thuan 1984; Klein, Weiland, & Brinks 1991). Low-metallicity BCDs also tend to be of low mass. Hence, they may represent the primordial “building blocks” – or “sub-galaxies” (Rees 1998) – in hierarchical scenarios of galaxy formation. As such, the study of their radio properties can be useful to better understand primordial galaxies.

One of the best candidates for the primordial building-block status is SBS 0335–052. At  $Z \sim 1/41 Z_{\odot}$  (Melnick, Heydari-Malayeri, & Leisy 1992; Izotov et al. 1997), it is the lowest-metallicity star-forming galaxy known after I Zw 18 ( $Z \sim 1/50 Z_{\odot}$ ). Its mass in stars is  $\lesssim 10^7 M_{\odot}$  (Papaderos et al. 1998; Vanzì et al. 2000), and it is embedded in an HI cloud of  $\sim 2 \times 10^9 M_{\odot}$  (Pustilnik et al. 2001). To explore the radio properties of star formation in a chemically unenriched interstellar medium, and to better understand the nature of the starburst in SBS 0335–052, we have obtained Very Large Array (VLA) D-array observations at five continuum frequencies. In this paper, we first describe in some detail the extremely metal-poor BCD SBS 0335–052. We then present the new radio observations and their reduction and analysis in §3, together with a description of the optical-radio alignment. Models of the continuum emission and the results of the spectral fitting are discussed in §4 and §5, respectively. In §6 we examine the properties of the starburst in SBS 0335–052,

as inferred from our observations, and assess the nature of the non-thermal radio source. Finally, we discuss the possible implications of our results for primordial star formation.

## 2. SBS 0335–052

At  $Z/Z_{\odot} \sim 1/41$ , SBS 0335–052 is the lowest-metallicity galaxy in the Second Byurakan Survey (Markarian, Lipovetskii, & Stepanian 1983). SBS 0335–052 comprises six main star clusters surrounded by a very blue ( $V - I = -0.3 - 0.2$ ) low-surface brightness diffuse component which, because of its filamentary structure and color, is almost certainly gas (Thuan, Izotov, & Lipovetsky 1997; Papaderos et al. 1998). It is more distant (redshift distance is 54.3 Mpc), and fainter ( $V = 16.65$ ) than I Zw 18, but more luminous ( $M_B = -16.7$ , Thuan, Izotov, & Lipovetsky 1997). SBS 0335–052 has a companion of similar metal abundance  $\sim 20$  kpc to the west, and both are embedded within a common HI cloud (Pustilnik et al. 2001). An HST (F791W) image of SBS 0335–052 is shown in Fig. 1.

The star clusters in SBS 0335–052 are sufficiently compact (diameter upper limit  $\leq 50$  pc) and luminous ( $-14.1 \leq V \leq -11.9$ ) to be defined as Super Star Clusters (SSCs) (Thuan, Izotov, & Lipovetsky 1997). Massive star density in the SSCs is  $\gtrsim 2.5 \text{ pc}^{-2}$ , with a high surface brightness  $\lesssim 16 \text{ mag arcsec}^{-2}$  in  $K$  for the two brightest SSCs (Vanzi et al. 2000). Optical spectra of SBS 0335–052 show evidence for Wolf-Rayet stars (Guseva, Izotov, & Thuan 2000), and a high electron temperature (20000–22000 K) and density ( $500\text{--}600 \text{ cm}^{-3}$ , Izotov et al. 1999).

Extinction as measured from the optical hydrogen recombination lines in the brightest SSC pair is  $A_V = 0.55$  mag (Izotov et al. 1997), but somewhat higher if measured with  $\text{Br}\gamma$ :  $A_V = 0.73$  mag (Vanzi et al. 2000). Extinction is higher still if measured with  $\text{Br}\alpha$  ( $\text{H}\beta/\text{Br}\alpha$ :  $A_V = 1.5$  mag;  $\text{Br}\gamma/\text{Br}\alpha$ :  $A_V = 12.1$  mag; Hunt, Vanzi, & Thuan 2001). Such high extinction appears to be caused by warm dust whose emission has been measured in the mid-infrared with the Infrared Space Observatory (Thuan, Sauvage, & Madden 1999) and from the ground (Dale et al. 2001). The warm dust emitting in the mid-infrared is associated with the two brightest SSCs, and resides in a region no more than 80-100 pc in diameter (Hunt, Vanzi, & Thuan 2001; Dale et al. 2001); the dust mass is  $\lesssim 10^5 M_{\odot}$  (Plante & Sauvage 2002). The SFR as derived from the integrated  $\text{H}\alpha$  emission is  $0.4 M_{\odot}/\text{yr}$  (Thuan, Izotov, & Lipovetsky 1997), while from the  $\text{Br}\alpha$  luminosity in the spectroscopic slit alone is  $1.7 M_{\odot}/\text{yr}$  (Hunt, Vanzi, & Thuan 2001). Those authors concluded that optical observations do not detect roughly 3/4 of the star formation in the brightest SSCs, and even  $2\mu\text{m}$  observations miss half of it.

### 3. VLA Observations and Data Reduction

Exploratory observations of SBS 0335–052 were taken on 9 November 2001 in D array at 8.4 GHz resulting in a detection of SBS 0335–052 in 3.5 hours of observation. A second round of observations at 1.4, 4.8, 8.5, 15 and 22 GHz were taken on 9 January 2002 during D→A move. While no source was detected at 1.4 GHz in 10 minutes, Dale et al. (2001) report a detection of SBS 0335–052 at  $3\sigma$  in a 1994 observation. We requested and received discretionary observing time on 12 September 2003 during the A→BnA move to confirm this detection and detected SBS 0335–052 at the  $7\sigma$  level.

There is no conclusive evidence that SBS 0335–052 is resolved in this  $1.6'' \times 1.5''$  resolution image, and we therefore assume it is unresolved in the images made with a larger beam at other frequencies. This assumption is corroborated by the excellent agreement of our A→BnA flux ( $0.47 \pm 0.06$  mJy/beam) and that obtained by Dale et al. (2001) at 1.49 GHz (0.40 mJy/beam) with a  $6''$  beam in the B configuration. Table 1 gives the fluxes, their uncertainties, the beam sizes and position angle, and the integration time of each observation. The uncertainty on the flux given in Table 1 includes the rms noise and 5% flux calibration uncertainty.

Table 1. VLA Observations of SBS 0335–052

Frequency [GHz]	Flux [mJy beam <sup>-1</sup> ]	Beam	Time on source
1.46	0.4571 ± 0.0610	1.6'' × 1.5'', 49°	45m
4.86	0.7720 ± 0.0855	29'' × 16'', 54°	12m
8.46	0.6508 ± 0.0386	12'' × 9'', -7°	3.5h
14.94	0.3960 ± 0.0704	12'' × 5'', 54°	1.8h
22.46	0.4817 ± 0.0789	6'' × 4'', 52°	1.3h

### 3.1. Optical-Radio Alignment

The radio source in our highest-resolution ( $1.5'' \times 1.6''$ ) image at 1.46 GHz is shown in Figure 1. The radio contours in units of  $\sigma$  are overlaid on the HST/WFPC2 image (Thuan, Izotov, & Lipovetsky 1997) in the F791W filter which we obtained from the HST archive and re-reduced. We performed our own astrometrical calibration using stars from the U.S. Naval Observatory Astrometric Catalog A2.0 (USNOA2.0<sup>1</sup>). In the  $1600 \times 1600$  pixel WFPC2 image, there are five stars in the USNOA2.0. The astrometric solution for the image, based on these stars, was calculated with the *imwcs* routine in the WCSTools package (available from <http://tdc-www.harvard.edu/software/wcstools/>). The solution has an rms uncertainty of  $0.54''$ , or roughly 5 WFPC2 (mosaic) pixels.

The correct HST/WFPC2 astrometry results in a virtually perfect alignment of the compact 20 cm radio source with the brightest SSCs (1 + 2) toward the southeast edge of SBS 0335–052. To the level of  $\sim 60 \mu\text{Jy}/\text{beam}$ , there is no significant radio emission coming from the other SSCs or the low-surface brightness envelope surrounding the star clusters.

## 4. Models for the Radio Spectrum

The radio continuum spectrum of SBS 0335–052 is nearly flat with a small negative slope for  $\nu > 5$  GHz, and a drop-off at  $\nu = 1.4$  GHz (Figure 2); the low-frequency drop-off is a signature of free-free absorption. The apparent spectral index of  $-0.4$  of the four points with  $\nu > 1.4$  GHz is similar to that obtained for a large sample of BCDs (Klein, Wielebinski, & Thuan 1984) ( $\alpha$  from 1.4–5 GHz =  $-0.33$ ), implying that absorption in most other BCDs must be less than in SBS 0335–052. The apparent spectral index is also steeper than optically thin thermal emission, implying that there must be some non-thermal contribution to the observed flux.

Because of the low-frequency drop, we did not attempt to fit the radio spectrum of SBS 0335–052 with the simplest model of combined thermal+non-thermal emission with no absorption (c.f., Klein, Weiland, & Brinks 1991). The models we investigated include thermal and non-thermal components, and the effects of free-free absorption from ionized

---

<sup>1</sup><http://tdc-www.harvard.edu/software/catalogs/ua2.html>

gas with several geometries. If  $\tau_{\text{ff}}$  is the free-free absorption optical depth <sup>2</sup>:

$$\tau_{\text{ff}} \simeq 0.08235 \left(\frac{T}{K}\right)^{-1.35} \left(\frac{EM}{\text{pc cm}^{-6}}\right) \left(\frac{\nu}{\text{GHz}}\right)^{-2.1} \quad (1)$$

where  $\nu$  is the frequency,  $T$  is the ionized gas temperature, and  $EM$  is the emission measure, the optically thin thermal emission  $f^{\text{th}}$  can be written as:

$$f_{\nu}^{\text{th}} = \phi (5.95 \times 10^{-5}) \left(\frac{T}{K}\right)^{-0.35} \left(\frac{\nu}{\text{GHz}}\right)^{-0.1} \left(\frac{EM}{\text{pc cm}^{-6}}\right) \left(\frac{\theta}{''}\right)^2 \text{ mJy} \quad (2)$$

$\phi$  is a geometrical factor that is equal to  $\pi/6$  for a spherical region of constant density and diameter  $\theta$ , and  $\pi/4$  for a cylindrical region of diameter and length  $\theta$  (e.g., Mezger & Henderson 1967).  $\phi$  also includes the filling factor, which we have assumed equal to unity. The non-thermal emission can be written as:

$$f_{\nu}^{\text{nt}} = f_{\nu_0}^{\text{nt}} \left(\frac{\nu}{\nu_0}\right)^{\alpha_{\text{nt}}} \text{ mJy} \quad (3)$$

where  $f_{\nu_0}^{\text{nt}}$  is the non-thermal (unabsorbed) flux at  $\nu_0$ . Model 1 includes absorption in the form of a foreground screen of ionized gas that obscures both thermal and non-thermal components:

$$f_{\nu}^{\text{tot}} = \exp(-\tau_{\text{ff}})(f_{\nu}^{\text{nt}} + f_{\nu}^{\text{th}}) \text{ mJy} \quad (4)$$

Model 2 assumes that the absorbing medium is intermixed with both thermal and non-thermal emission:

$$f_{\nu}^{\text{tot}} = \left[\frac{1 - \exp(-\tau_{\text{ff}})}{\tau_{\text{ff}}}\right] (f_{\nu}^{\text{nt}} + f_{\nu}^{\text{th}}) \text{ mJy} \quad (5)$$

Model 3 includes a screen absorption term only for the non-thermal component, while the absorbing medium is assumed to be homogeneously intermixed with the thermal emission:

$$f_{\nu}^{\text{tot}} = \exp(-\tau_{\text{ff}}) f_{\nu}^{\text{nt}} + \left[\frac{1 - \exp(-\tau_{\text{ff}})}{\tau_{\text{ff}}}\right] f_{\nu}^{\text{th}} \text{ mJy} \quad (6)$$

These models represent slightly different geometries. In models 1 and 2, thermal and non-thermal regions are assumed to be cospatial. In model 3, the absorbing medium and thermal emitting region must lie between the non-thermal emission and the telescope, or “outside” of it. Models in which the non-thermal emission was not absorbed, for example when the non-thermal source is more extended than the thermal emitter/absorber, give significantly worse fits than the three models considered here.

---

<sup>2</sup>This approximation for  $\tau_{\text{ff}}$  is accurate to  $\lesssim 20\%$ .

We fit the VLA spectrum to these models using a  $\chi^2$  minimization technique to estimate  $f_{\nu_0}^{\text{nt}}$ ,  $\theta$ , and  $EM$  (through  $\tau_{\text{ff}}$ ) based on the *amoeba* algorithm (Press et al. 1992). Errors for the fitted parameters were obtained according to the precepts of Lampton, Margon, & Bowyer (1976) for three fitted parameters and a confidence level of 95%.  $\nu_0$  was chosen to be 5 GHz.  $\alpha_{\text{nt}}$  was fixed *a priori* to  $-0.8$ , although values ranging from  $-0.5$  to  $-1.1$  did not affect the relative quality of the fits (but see §5). The electron temperature  $T_e$  was taken to be 20000 K (Izotov et al. 1999). We have tested our fitting procedure against Deeg et al. (1993) for II Zw 40, and obtain results consistent with theirs.

#### 4.1. Additional Physical Processes

In addition to the models already described, we also investigated other physical mechanisms that may help shape the radio spectrum of SBS 0335–052.

Since the ultraviolet (UV) radiation field in SBS 0335–052 is roughly 10000 times the local value (Dale et al. 2001), inverse Compton losses may be important. Following Deeg et al. (1993), we included this effect in the expression for the non-thermal spectrum. These fits gave a larger  $\chi^2$ , probably because of the insensitivity of the spectrum to the non-thermal emission, given the dominant thermal emission at high frequencies in SBS 0335–052.

We also investigated the possible effect of a thermal plasma in the synchrotron emission region. This effect, usually called the Razin-Tsytoich effect (e.g., Simon 1969), does not appear to influence the shape of SBS 0335–052’s radio spectrum. For SBS 0335–052, the Razin-Tsytoich cutoff frequency appears to be less than the thermal cutoff, since we were unable to obtain good fits by including this effect. This would be the case if the magnetic field  $B > 4 \times 10^{-5}/\sqrt{L}$  where  $L$  is the physical dimension of the emitting region in pc (see Verschuur & Kellermann 1988). For  $L = 30$  pc,  $B > 7 \mu\text{G}$ . The equipartition magnetic field inferred from our observations (see §5) is more than 100 times this value.

### 5. Spectral Fitting Results

For  $\alpha = -0.8$ , the best fit for each of the three models gave a similar minimum of reduced  $\chi_{\nu}^2 = 1.6$ . Nominally, the best fit was obtained with the mixed geometry for both components (model 2), but the lowest  $\chi_{\nu}^2 = 1.60$  was only slightly lower than that obtained with screen geometry for one or both of the components (models 1 and 3:  $\chi_{\nu}^2 = 1.67$ ). The best-fit models together with the observed spectrum are shown in Fig. 2. With model 2 (mixed geometry, left panel of Fig. 2), assuming a spherical geometry and  $\alpha_{\text{nt}} = -0.8$ , the



best-fit parameters are:

$$EM = (7.6 \pm 2.9) \times 10^7 \text{ pc cm}^{-6} \quad (7)$$

$$\theta = 0.063 \pm 0.001 \text{ arcsec} \quad (8)$$

$$f_{\nu_0}^{\text{nt}} = 0.68 \pm 0.007 \text{ mJy} \quad (9)$$

The resulting mean-square residuals are 0.06 mJy, averaged over the 5 data points. The thermal fraction at 5 GHz is 0.27, which gives a 5 GHz thermal flux of 0.25 mJy. With model 3 (screen absorption for non-thermal, mixed for thermal, right panel of Fig. 2) and a spherical geometry and  $\alpha_{\text{nt}} = -0.8$ , the best-fit parameters are:

$$EM = (2.8 \pm 0.8) \times 10^7 \text{ pc cm}^{-6} \quad (10)$$

$$\theta = 0.11 \pm 0.01 \text{ arcsec} \quad (11)$$

$$f_{\nu_0}^{\text{nt}} = 0.60 \pm 0.005 \text{ mJy} \quad (12)$$

The thermal fraction at 5 GHz is 0.32, which gives a 5 GHz thermal flux of 0.29 mJy. Again, the resulting mean-square residuals are 0.06 mJy.

There is an indication that the non-thermal spectral index is steeper than the canonical  $\alpha = -0.8$ , since the lowest value of  $\chi_{\nu}^2$  (1.37) was obtained with model 2 by fixing  $\alpha = -1.6$ . However, while this result is formally a slightly better fit than that we obtain with  $\alpha = -0.8$ , with such a steep  $\alpha$  the other geometries give substantially worse fits. Unlike steeper indices,  $\alpha = -0.8$  gives similarly low  $\chi_{\nu}^2$  also for the different absorption geometries. We therefore chose to fix  $\alpha = -0.8$ .

Our data are unable to distinguish among the various absorption geometries (screen, mixed, or combined), although a screen absorption of both thermal and non-thermal components is physically unrealistic. Lower frequency observations would be necessary to distinguish the models (see Fig. 2). In what follows, we therefore consider the range of the best-fit values implied by the mixed/combined geometries (models 2 and 3). The non-thermal fraction and flux levels do not vary much with geometry (0.68–0.73, 0.60–0.68 mJy, respectively), but the thermal emission measure and source size change by a factor of two or more.

### 5.1. Thermal Emission

The fitted diameter of the thermal emission region  $\theta$  corresponds to a physical size  $D = 17 - 29 \text{ pc}$ , several times smaller than the 80 pc diameter from Dale et al. (2001) and the outer radius of 110 pc predicted by the dust model of Plante & Sauvage (2002). Given  $\theta$ ,

the global  $EM$  determined from our fit can be used to estimate the ionized gas density  $n_e$ . The resulting densities  $n_e$  range from 980–2100  $\text{cm}^{-3}$ . These values are higher than those inferred from optical spectroscopy  $n_e \gtrsim 600 \text{ cm}^{-3}$  (Izotov et al. 1999). However in the optical we cannot probe very far into the star clusters; hence the density could easily be higher than optical estimates. Also, the optical spectroscopy is averaged over a larger region ( $\gtrsim 260 \text{ pc}$ ) than the size we infer from our fit.

The best-fit emission measure of  $2.8 - 7.6 \times 10^7 \text{ pc cm}^{-6}$  is not an extreme value for dwarf starburst galaxies. In He 2-10 and NGC 5253, emission measures range from  $10^7$  to  $10^8 \text{ pc cm}^{-6}$  and implied densities between  $500 < n_e < 10^4 \text{ cm}^{-3}$ . (Kobulnicky & Johnson 1999; Mohan, Anantharamaiah, & Goss 2001). In Wolf-Rayet galaxies, typical emission measures are  $10^8 - 10^9 \text{ pc cm}^{-6}$ , with densities  $\gtrsim 10^3 \text{ cm}^{-3}$  (Beck, Turner, & Kovo 2000). In II Zw 40, another BCD, Beck et al. (2002) deduce an  $EM$  of  $10^9 \text{ pc cm}^{-6}$  for the most compact sources.

## 5.2. Non-Thermal Emission

Above 1.4 GHz, the apparent spectral index is  $-0.4$ , a clear indicator of significant non-thermal emission. Indeed, the fitted fraction of non-thermal radio emission at  $\nu = 5 \text{ GHz}$  is 0.7, with a 5 GHz non-thermal flux  $f_{\nu_0}^{\text{nt}} = 0.60 - 0.68 \text{ mJy}$ . We can use  $f_{\nu_0}^{\text{nt}}$  to estimate the magnetic field strength in SBS 0335–052, assuming equipartition between the magnetic field energy and the energy of the relativistic particles (Pacholczyk 1970). We take the ratio of relativistic proton to electron energies to be  $k = 40$  (e.g., Deeg et al. 1993), assume a spherical volume of diameter 17-29 pc with unit filling factor, and a constant spectral index from  $\nu_1 = 10^7 \text{ Hz}$  to  $\nu_2 = 10^{11} \text{ Hz}$ . We obtain a synchrotron luminosity<sup>3</sup>  $L_{\text{syn}} = 8 - 9 \times 10^{37} \text{ erg s}^{-1}$ , and an equipartition  $B = 633 - 1065 \mu\text{G}$ , an extremely high value for magnetic field strength. The corresponding minimum pressure within the synchrotron emitting region is  $3 \times 10^{-8} - 1 \times 10^{-7} \text{ dyne cm}^{-2}$ , and the equipartition energy is  $\sim 10^{52} \text{ erg}$ . These values, although extreme, are similar to the magnetic field strength and pressure estimated for the compact sources in M 82 (Allen & Kronberg 1998).

Although magnetic fields in very active star-forming galaxies tend to be much stronger than in less active galaxies such as the Milky Way (Kronberg, Lesch, & Hopp 1999), we cannot be certain that such a high value for the magnetic field in SBS 0335–052 is correct. First, the source may be too young to have achieved the minimum-energy configuration (see

---

<sup>3</sup> $L_{\text{syn}}$  is the total synchrotron luminosity obtained by integrating the non-thermal spectrum from  $\nu_1 = 10^7 \text{ Hz}$  to  $\nu_2 = 10^{11} \text{ Hz}$ .

§6.4). Second, the standard formula for magnetic field strength relies on a fixed integration interval in frequency. In the case of SBS 0335–052, with its relatively high non-thermal radio luminosity, this procedure is almost certainly inappropriate. A fixed frequency interval corresponds to different electron energy intervals, because of the dependence on magnetic field strength (Beck et al. 1996). Using the correct formula, and integrating from a proton energy of 300 MeV to infinity, we obtain an equipartition field of  $30 \mu\text{G}$  (R. Beck, private communication), similar to the field strengths of other BCDs (Deeg et al. 1993).

## 6. Radio Emission and Star Formation in SBS 0335–052

The results from the spectral fits allow us to separate thermal and non-thermal emission in SBS 0335–052. From the thermal emission, we can then derive the number of ionizing photons, the star-formation rate, and the supernova rate.

### 6.1. Ionizing Photons

With a thermal flux of  $0.25 - 0.29 \text{ mJy}$  at  $5 \text{ GHz}$ , the inferred thermal luminosity  $L_{\text{T}} = 8.8 \times 10^{19} - 1.0 \times 10^{20} \text{ W Hz}^{-1}$ . Because of the high electron temperature in SBS 0335–052, the usual scaling for ionizing photons (e.g., Rubin 1968; Caplan & Deharveng 1986; Lequeux 1980; Condon 1992) give inconsistent results. We therefore provide in the Appendix a new set of relations which are valid to within 0.5% for  $10000\text{K} \leq T \leq 20000\text{K}$ . These are useful for comparing thermal radio emission and optical/near-infrared recombination lines in low-metallicity high temperature environments, and we use them here. With this thermal luminosity, Equation A6 gives the number of ionizing photons  $N_{\text{ion}} = 8.2 - 9.4 \times 10^{52} \text{ photons s}^{-1}$ . With 1 O7V star =  $10^{49} \text{ photons s}^{-1}$  (Leitherer 1990), we obtain  $\sim 9000$  equivalent O7 stars.

From the  $\text{Br}\alpha$  line luminosity of  $3.2 \times 10^{39} \text{ erg s}^{-2}$  (Hunt, Vanzi, & Thuan 2001) *uncorrected for extinction*, with  $T = 20000\text{K}$ , we infer a total of 19400 stars. A correction for a screen extinction of  $A_V \gtrsim 12$  (Hunt, Vanzi, & Thuan 2001; Plante & Sauvage 2002) would increase these values by a factor of 1.6, a mixed geometry correction a factor of 2.4. It is clear that the  $\text{Br}\alpha$  is powered by between two and five times the ionizing photons responsible for the thermal radio emission.

Either our estimate of the thermal fraction is wrong, or there is a source of ionized gas emission in addition to the HII region associated with the SSCs. The apparent spectral index  $\alpha$  of  $-0.4$  is indicative of a substantial non-thermal component as mentioned before, and is also implied by our spectral fits. Even if the entire observed  $5 \text{ GHz}$  flux ( $0.8 \text{ mJy}$ ) were

thermal, a reasonable extinction correction for the Br $\alpha$  emission would still give a similar discrepancy. We therefore favor the hypothesis of an additional source of ionized gas, namely an extended envelope of ionized gas resulting from massive stellar winds. Such winds are known to exist in SBS 0335–052 from its UV spectrum which shows strong Si IV 1394, 1403 absorption lines with the characteristic P-Cygni profiles (Thuan & Izotov 1997).

## 6.2. The Stellar Wind

To account for the presence of an extended stellar wind in SBS 0335–052, we performed a new set of spectral fits which included the spectrum of free-free radiation from varying-density envelopes (Panagia & Felli 1975), in addition to the thermal and non-thermal components described above. Traditional HII region constant density models do not fit such regions because of the different spectral behavior ( $f_\nu \propto \nu^{0.6}$ ). Physically, such a configuration could occur if there were a density-bounded inner wind zone optically thick in the radio, but not in Br $\alpha$ , surrounded by an HII region. The  $\chi_\nu^2$  from these new fits are formally equivalent to the best-fit models of §5, although the influence of the wind in the radio spectrum would not be apparent in Fig. 2, because of the low amplitude of the wind relative to the other components. The best-fit model gives the fraction of the wind contribution at 5 GHz as 0.004, which corresponds to an 8.5 GHz flux of 0.0035 mJy. With a cluster the size of that inferred in §6.1, this would correspond to a stellar wind of the order of  $\dot{M}_\odot \sim (v_\infty/1000 \text{ km s}^{-1}) 1 \times 10^{-4} M_\odot \text{ yr}^{-1}$  per star (e.g., Lang, Goss, & Rodríguez 2001), where  $v_\infty$  is the stellar wind’s terminal velocity. This velocity being about 500 km s $^{-1}$  in SBS 0335–052 (Thuan & Izotov 1997),  $\dot{M}_\odot$  is roughly  $5 \times 10^{-5} M_\odot \text{ yr}^{-1}$ . This is not an unreasonable value compared to observed values for late-type WN stars (Leitherer et al. 1997) or for massive stars in the Galactic center (Lang, Goss, & Rodríguez 2001).

We can predict how much Br $\alpha$  flux we would expect from a stellar wind with the radio properties of SBS 0335–052. Using the formalism in Simon et al. (1983), and assuming that Br $\alpha$  is optically thick<sup>4</sup>, we would expect  $3.2 \times 10^{-14} \text{ erg cm}^{-2} \text{ s}^{-1}$ , several times higher than the observed Br $\alpha$  flux of  $9.0 \times 10^{-15} \text{ erg cm}^{-2} \text{ s}^{-1}$  (Hunt, Vanzi, & Thuan 2001). An extinction correction for mixed geometry ( $\tau_{\text{Br}\alpha} = 2.1$ ) would give a flux of  $2.3 \times 10^{-14} \text{ erg cm}^{-2} \text{ s}^{-1}$ , lower than, but comparable to, the wind prediction. The radio emission from the wind may be overestimated by our fit, and the extinction correction for Br $\alpha$  uncertain, but the wind+ HII-region model seems to be able to account for the Br $\alpha$  flux better than

---

<sup>4</sup>If the Br $\alpha$  flux were optically thin, the predicted flux would be  $10^5$  times higher than observed. Also, these calculations assume an electron temperature of 10000 K.

the HII-region model alone.

The radio contribution from the HII region is far larger than that from the stellar wind, while the Br $\alpha$  emission is much stronger from the wind than from the HII region. The Br $\alpha$  flux inferred from the thermal radio continuum,  $3.7 \times 10^{-15} \text{ erg cm}^{-2} \text{ s}^{-1}$ , is a factor of  $\sim 10$  times lower than what we would expect from an optically thick wind (see above). Moreover, it is less than half the observed value of  $9.0 \times 10^{-15} \text{ erg cm}^{-2} \text{ s}^{-1}$ , which is a lower limit because of the extinction correction. It is evident that in SBS 0335–052 there is an excess of Br $\alpha$  flux over what we would expect from a simple HII region. The hot massive stars of the Arches Cluster in the Galactic Center show a similar, if more extreme, excess; comparing the radio emission (Lang, Goss, & Rodríguez 2001) to the near-infrared recombination line flux (Nagata et al. 1995) shows that the Br $\alpha$  luminosity is more than 20 times greater than expected from a Case B HII region extrapolated from the radio.

### 6.3. Star-Formation Rate

The thermal radio emission can also be used to derive the massive star-formation rate (SFR). First, using the formulation given in the Appendix, valid for high temperatures, and assuming that  $N(\text{He}^+)/N(\text{H}^+) = 0.08$ ,  $T = 20000\text{K}$ , and  $f_{\text{H}\alpha}/f_{\text{H}\beta} = 2.75$ , from  $L_{\text{T}}$  we derive the H $\alpha$  luminosity  $L_{\text{H}\alpha} = 5.8 - 6.7 \times 10^{40} \text{ erg s}^{-1}$ . Then, following Condon (1992), we estimate the SFR of stars more massive than  $5 M_{\odot}$   $\text{SFR}_{\geq 5 M_{\odot}} = 0.13 - 0.15 M_{\odot} \text{ yr}^{-1}$ .

The *total* SFR including less massive stars is  $0.7 - 0.8 M_{\odot} \text{ yr}^{-1}$ , about half the value estimated by Hunt, Vanzi, & Thuan (2001). The reason for this is that the near-infrared recombination line flux is apparently partly due to stellar winds; consequently, numbers of massive stars and star-formation rates inferred from the near-infrared recombination lines are overestimated.

We can infer the total stellar mass in the cluster, assuming an age and a population synthesis model. For an age of 5 Myr (Papaderos et al. 1998; Vanzi et al. 2000), and with Starburst 99 (Leitherer et al. 1999), the number of O7V stars given by the thermal radio luminosity in SBS 0335–052 corresponds to a total stellar mass of  $2.4 \times 10^6 M_{\odot}$ . This is very close to the total stellar mass of  $2 \times 10^6 M_{\odot}$  estimated by Plante & Sauvage (2002) on the basis of the integrated infrared spectral energy distribution, but is 3 times lower than that of Hunt, Vanzi, & Thuan (2001). Again, this last discrepancy is because of the Br $\alpha$  excess described above.

#### 6.4. Non-thermal Radio Emission and Supernovae

Non-thermal radio emission can be used to estimate the star-formation rate in SBS 0335–052, provided it follows usual scaling relations (e.g., Condon 1992). Here we investigate this assumption, and use our observations to determine the origin of the non-thermal radio emission in SBS 0335–052.

Given the  $\text{SFR}_{\geq 5 M_{\odot}}$ , we can estimate the supernova (SN) rate  $\nu_{\text{SN}}$ . Almost independently of the form of the initial mass function,  $\nu_{\text{SN}} = 0.041 \text{ SFR}_{\geq 5 M_{\odot}} \text{ yr}^{-1}$ . With  $\text{SFR}_{\geq 5 M_{\odot}} = 0.13 - 0.15 M_{\odot} \text{ yr}^{-1}$ ,  $\nu_{\text{SN}} = 0.005 - 0.006 \text{ yr}^{-1}$ . This is only 3–4 times smaller than the recent estimate of  $0.016 \text{ yr}^{-1}$  for M 82 (Allen & Kronberg 1998), and the Type II SN rate of the Galaxy,  $0.023 \text{ yr}^{-1}$  (Tammann 1982), which however are galaxies over 1000 times more massive. We can also use the relations given in Condon (1992) for normal galaxies to deduce the non-thermal radio luminosity  $L_{\text{NT}}$  we would expect from a typical starburst with this  $\nu_{\text{SN}}$ . In SBS 0335–052, predicted  $L_{\text{NT}}$  is  $1.9 - 2.2 \times 10^{20} \text{ W Hz}^{-1}$ , corresponding to an expected non-thermal flux  $f_{\nu_0} \approx 0.6 \text{ mJy}$  at 5 GHz. This value is very close to the model fit value of 0.60–0.68 mJy at 5 GHz.

It is puzzling why the scaling relation derived for massive spiral galaxies with evolved starbursts (e.g., Condon & Yin 1990) would hold for SBS 0335–052. Non-thermal radio emission in spiral galaxies is almost certainly produced by relativistic electrons diffusing over the galactic disk. The timescale for this diffusion on kpc scales is  $10^7 - 10^8 \text{ yr}$  (Helou & Bica 1993). As noted by Condon (1992), although SNe almost certainly accelerate initially the electrons responsible for non-thermal emission we observe, >90% of it was produced long after the discrete SNe have faded out. The starburst in SBS 0335–052 is very young, 5 Myr or younger (Vanzi et al. 2000). It therefore seems unlikely that the diffusion mechanism active in the majority of spiral galaxies has had enough time to operate in SBS 0335–052 to produce the observed amount of non-thermal emission.

The dimensions of the radio source as implied by the models are also inconsistent with the standard diffusion picture. The non-thermal source cannot be larger than the beam width (FWHM  $\sim 400 \text{ pc}$ ), and almost certainly is at least 10 times smaller than this given the constraints imposed by the spectral fit. This size is 50–100 times smaller than that of the diffuse kpc-scale radio emission mechanism which powers normal spiral galaxies.

We therefore investigate possible sources of non-thermal emission which are both spatially compact and develop on a short timescale. On the very shortest timescales ( $\lesssim 100 \text{ yr}$ ), the non-thermal radio emission in SBS 0335–052 could come from a single radio SN seen at a time not long after its explosion. The inferred  $L_{\text{NT}} = 2 \times 10^{20} \text{ W Hz}^{-1}$  is not unusual for radio SN (Weiler et al. 2002), but because of the rapid decline of radio emission on timescales

of decades, we must be observing it not long after it occurred. However, the lack of radio variability over the 9-yr period spanned by our observations and those in Dale et al. (2001) suggest that this interpretation may not be the best one.

Alternatively, on slightly longer timescales, the non-thermal radio emission in SBS 0335–052 could arise either from radio SNe or evolved SN remnants. Radio SNe have adiabatic lifetimes of  $\sim 2 \times 10^4$  yrs (Woltjer 1972), and from the  $\nu_{\text{SN}}$  derived above, we can estimate the radio luminosity we would expect from a population of these (e.g., Ulvestad 1982). From radio SNe that emit only during the adiabatic phase of their evolution, we would expect at 5 GHz  $L_{\text{NT}} = 3.5 \times 10^{19} \text{ W Hz}^{-1}$ ; this is *6 times smaller* than the observed  $L_{\text{NT}} = 1.9\text{--}2.2 \times 10^{20} \text{ W Hz}^{-1}$  at 5 GHz. The non-thermal source in SBS 0335–052 is therefore difficult to interpret as an ensemble of standard radio SNe.

Finally, the radio source in SBS 0335–052 could be interpreted as one or more evolved compact SN remnants similar to those observed in M 82 (Allen & Kronberg 1998). As proposed by Chevalier & Fransson (2001), such remnants could be interacting with a dense interstellar medium, with  $n_e \sim 10^3 \text{ cm}^{-3}$ , similar to the  $n_e$  we derive for SBS 0335–052. The timescales for this radiative phase are longer than the pure adiabatic lifetimes (Chevalier & Fransson 2001), and, given the intense starburst and massive SSCs in SBS 0335–052, we could expect to detect sources with properties similar to those in M 82. Since  $\nu_{\text{SN}}$  in SBS 0335–052 corresponds to roughly 1 SN every 54 yr, it would not be unlikely for a few of these to be visible at the current epoch. As mentioned before, the equipartition pressure and magnetic field in SBS 0335–052 are similar to those in M 82. The physical dimensions of such compact sources are  $\lesssim 4 \text{ pc}$  (Muxlow et al. 1994), so they could conceivably reside inside the 30 pc diameter region responsible for the thermal emission and absorption. The non-thermal flux of SBS 0335–052 placed at the 3.63 Mpc distance of M 82 would be  $\sim 130 \text{ mJy}$ , similar to the flux of the most luminous of M 82’s compact sources, and equivalent to the flux of a few to ten or so of the less luminous ones.  $L_{\text{syn}}$  in SBS 0335–052 is only 4 times higher than the most luminous source in M 82, and comparable to the predictions of Chevalier & Fransson (2001). We conclude that a few compact evolved remnants, similar to those observed in M 82 as well as other starbursts (e.g., Smith et al. 1998), could be responsible for the non-thermal radio emission in SBS 0335–052. VLBI and high-resolution X-ray observations are necessary to verify this hypothesis.

Indeed, Chandra observations of SBS 0335–052 show evidence for a compact point source roughly spatially coincident with the compact non-thermal radio source we find here, and associated with the two brightest SSCs (Thuan et al. 2003). The X-ray source is extremely luminous in the 0.5–8.0 keV range ( $3 \times 10^{39} \text{ erg s}^{-1}$ ), and would be classified as an ultra-luminous X-ray source (ULX) if it is a single object.

The nature of the radio+X-ray emitting object is however not clear. Whether the X-ray source is a single ULX or several high-mass X-ray binaries (HMXRBs) is impossible to judge with the Chandra resolution. But while there are more than a hundred HMXRBs in our Galaxy (Liu, van Paradijs, & van den Heuvel 2000), only  $\leq 5\%$  of these are radio emitters (Clark et al. 2001). Although the X-ray luminosity is similar to that expected from a microquasar associated with a medium-mass black hole, its radio luminosity well exceeds (by  $10^6$ ) that observed in other such objects (Mirabel & Rodríguez 1998). Also its non-thermal radio spectrum is much steeper than the flat spectra thought to be characteristic of black hole systems in the low/hard spectral state (Martí et al. 2002). Moreover, as mentioned above, there is no evidence for either radio variability over a 9-yr interval or X-ray variability over shorter timescales, although the limited photon statistics do not strongly constrain the temporal nature of the X-ray source (Thuan et al. 2003). Hence, the radio source and the X-ray one could be physically distinct objects, the non-thermal radio luminosity coming from evolved SNRs expanding in a dense medium, and the X-ray luminosity from a single ULX or several HMXRBs. Independently of the specific nature of the compact object(s) responsible for the X-ray and radio emission, it is evident that they are connected to the SSCs and the starburst episode which formed them.

### 6.5. Implications for High-Redshift Star Formation

There are two noteworthy features of the radio continuum in SBS 0335–052, relative to spectra of normal spiral galaxies or other BCDs. First, there is significant free-free absorption on a global scale, of sufficient amplitude to suppress by a factor of 4 or more the observed flux at 1.49 GHz. Second, while the spectrum of SBS 0335–052 is significantly different from those of normal spirals, it is not completely thermal as in other BCDs. At 5 GHz, we find roughly a 30-70 mix of thermal and non-thermal emission.

If SBS 0335–052 can be taken as representative of star formation in an extremely low-metallicity environment, care should be taken when deriving cosmological conclusions from present and future radio continuum surveys. Because of the young age, low metal abundance, and intensity of the starburst, galaxies like SBS 0335–052 may not obey the usual scaling laws laid out in Condon (1992). Moreover, the effects of free-free absorption substantially alter the spectrum at frequencies  $\lesssim 1.5$  GHz. It would not be straightforward to disentangle such an effect when deriving the SFR as a function of redshift. Young starbursts occurring in a metal-poor, but dusty and dense environment, have integrated radio properties that may be very different from those of evolved starburst prototypes such as M 82 and Arp 220. As a result, photometric redshifts inferred from “standard” spectral-energy distributions could



also be incorrect.

## 7. Summary and Conclusions

We have presented new VLA continuum observations of the extremely metal-poor BCD SBS 0335–052, and fit the spectrum to a variety of models.

- The best-fitting model (model 2), which assumes an absorption medium intermixed with thermal+non-thermal emission, gives an  $EM = 7.6 \times 10^7 \text{ pc cm}^{-6}$  and a diameter of the radio-emitting region of 17 pc. The inferred density is  $n_e \sim 2000 \text{ cm}^{-3}$ .
- The non-thermal fraction at 5 GHz is 0.7, with an unabsorbed non-thermal 5 GHz flux of 0.68 mJy, corresponding to  $L_{\text{NT}} = 2.2 \times 10^{20} \text{ W Hz}^{-1}$ . From this, we derive an equipartition magnetic field of  $\sim 1 \text{ mG}$ , and a pressure of  $\sim 10^{-7} \text{ dyne cm}^{-2}$ . Integrating over a fixed electron energy interval, rather than one at fixed frequency, gives a field strength of  $30 \mu\text{G}$ .
- We find evidence for a stellar wind in SBS 0335–052, because of the excess of Br $\alpha$  flux over that inferred from the thermal radio emission.
- Because of the compact size and young age of the starburst, it is difficult to interpret the non-thermal radio emission as due to diffusion of SN-accelerated electrons on timescales of  $10^7 - 10^8 \text{ yr}$ . Rather, we attribute the non-thermal radio emission to an ensemble of compact SN remnants expanding in a dense interstellar medium.

KKD is supported by a National Science Foundation Astronomy and Astrophysics Postdoctoral Fellowship under award AST-0103879. TXT acknowledges the partial financial support of NSF grant AST-0205785. LKH would like to thank Rainer Beck, Riccardo Cesaroni, Dick Crutcher, and Marcello Felli for extremely enlightening discussions. This paper has made use of the astrometry package WCS Tools available from <http://td-www.harvard.edu/software/wcstools.html>.

### A. Ionizing Photons and Optical/Radio Ratio for Electron Temperatures > 10000 K

For a radiation-bounded HII region,

$$N_{\text{ion}} = \int n_e n(\text{H}^+) \alpha_B dV \quad (\text{A1})$$

where  $N_{\text{ion}}$  is the number of ionizing photons,  $n_e$  and  $n(\text{H}^+)$  are the electron and ionized hydrogen number densities respectively, and  $\alpha_B$  is the Case B recombination coefficient (Osterbrock 1989). Here, we have neglected the absorptions by He since they do not greatly reduce the number of photons available for ionizing H (Osterbrock 1989).

The radio free-free emissivity  $j_\nu$  can be written as:

$$4\pi j_\nu = 4.102 \times 10^{-39} \left( \frac{\nu}{\text{GHz}} \right)^{-0.1} \left( \frac{T}{10^4 \text{ K}} \right)^{-0.35} n_e [n(\text{H}^+) + n(\text{He}^+)] \quad (\text{A2})$$

in units of  $\text{erg s}^{-1} \text{ cm}^{-3} \text{ Hz}^{-1}$ , and where  $T$  is the electron temperature, and  $n(\text{He}^+)$  is the number density of ionized helium (Altenhoff et al. 1960; Mezger & Henderson 1967; Rubin 1968; Caplan & Deharveng 1986). The correction factor between this approximation and the more exact form given in Oster (1961) is 0.9975 for  $T = 20000 \text{ K}$  (see Mezger & Henderson 1967). Integrating  $4\pi j_\nu$  over the emitting volume and placing a source with this luminosity at distance  $d$  gives an expression for the radio flux:

$$f_\nu = 3.43 \times 10^{-63} \left( \frac{d}{\text{Mpc}} \right)^{-2} \left( \frac{\nu}{\text{GHz}} \right)^{-0.1} \left( \frac{T}{10^4 \text{ K}} \right)^{-0.35} \int n_e [n(\text{H}^+) + n(\text{He}^+)] dV \quad \text{mJy} \quad (\text{A3})$$

The temperature dependence of the recombination coefficient  $\alpha_B$  is very different for temperatures > 10000 K, than for cooler ones. If a power law approximation is assumed for this dependence, and using the values given by Osterbrock (1989), for  $T \text{ 10000 K} \leq T \leq 20000 \text{ K}$  we find:

$$\alpha_B = 2.59 \times 10^{-13} \left( \frac{T}{10^4 \text{ K}} \right)^{-0.04}. \quad (\text{A4})$$

By combining Equations A3 and A1, and eliminating the volume integrals, we can write the number of ionizing photons  $N_{\text{ion}}$  as a function of thermal free-free flux:

$$N_{\text{ion}} = 7.56 \times 10^{49} \left( \frac{d}{\text{Mpc}} \right)^2 \frac{n(\text{H}^+)}{n(\text{H}^+) + n(\text{He}^+)} \left( \frac{\nu}{\text{GHz}} \right)^{0.1} \left( \frac{T}{10^4 \text{ K}} \right)^{0.31} \left( \frac{f_\nu}{\text{mJy}} \right) \quad (\text{A5})$$

Except for the different temperature dependence, this equation is the same as Rubin (1968) and Lequeux (1980), but we have left explicit the effect of ionized He;  $n(\text{He}^+)/n(\text{H}^+)$  is

$\sim 0.08$  for low-metallicity environments (e.g., the Magellanic Clouds: Caplan & Deharveng 1986; SBS 0335–052: Melnick, Heydari-Malayeri, & Leisy 1992).

Equation A5 can also be expressed in terms of radio luminosity  $L_T$  rather than flux:

$$N_{\text{ion}} = 6.32 \times 10^{52} \frac{n(\text{H}^+)}{n(\text{H}^+) + n(\text{He}^+)} \left(\frac{\nu}{\text{GHz}}\right)^{0.1} \left(\frac{T}{10^4 \text{ K}}\right)^{0.31} \left(\frac{L_T}{10^{20} \text{ W Hz}^{-1}}\right) \quad (\text{A6})$$

Equation A6 is equivalent to that given by Condon (1992), except for the different temperature dependence and the explicit inclusion of the dependence on  $\text{He}^+$ ; our expression is valid for  $10000 \text{ K} \leq T \leq 20000 \text{ K}$ .

We now turn to the hydrogen recombination lines for  $10000 \text{ K} \leq T \leq 20000 \text{ K}$ . Using the coefficients in Osterbrock (1989), and assuming a power-law dependence on  $T$ , the (Case B)  $\text{H}\beta$  emissivity  $j_{\text{H}\beta}$  can be written as:

$$4\pi j_{\text{H}\beta} = 1.24 \times 10^{-25} n_e n(\text{H}^+) \left(\frac{T}{10^4 \text{ K}}\right)^{-0.91} \quad (\text{A7})$$

in units of  $\text{erg s}^{-1} \text{ cm}^{-3}$  (c.f., Mezger & Henderson 1967). As before, we integrate  $4\pi j_{\text{H}\beta}$  over the emitting volume to obtain the total  $\text{H}\beta$  luminosity  $L_{\text{H}\beta}$ , which, when combined with Eq. A1 and Eq. A4, gives the number of ionizing photons as a function of  $L_{\text{H}\beta}$ :

$$N_{\text{ion}} = 2.09 \times 10^{12} \left(\frac{T}{10^4 \text{ K}}\right)^{0.87} \left(\frac{L_{\text{H}\beta}}{\text{erg s}^{-1}}\right) \quad (\text{A8})$$

Placing this source at distance  $d$  gives an expression which depends on the  $\text{H}\beta$  flux  $f_{\text{H}\beta}$ :

$$N_{\text{ion}} = 2.50 \times 10^{50} \left(\frac{T}{10^4 \text{ K}}\right)^{0.87} \left(\frac{d}{\text{Mpc}}\right)^2 \left(\frac{f_{\text{H}\beta}}{10^{-12} \text{ erg cm}^{-2} \text{ s}^{-1}}\right) \quad (\text{A9})$$

The  $\text{H}\beta$  flux expected from the radio free-free emission is therefore given by:

$$\left(\frac{f_{\text{H}\beta}}{10^{-12} \text{ erg cm}^{-2} \text{ s}^{-1}}\right) = 0.302 \frac{n(\text{H}^+)}{n(\text{H}^+) + n(\text{He}^+)} \left(\frac{T}{10^4 \text{ K}}\right)^{-0.56} \left(\frac{\nu}{\text{GHz}}\right)^{0.1} \left(\frac{f_\nu}{\text{mJy}}\right) \quad (\text{A10})$$

Equation A10 is very similar to Condon (1992) because the different temperature dependence on the recombination coefficient used here disappears in the ratio.

Other recombination lines can be used if the temperature dependence is taken into account. Again, using the coefficients in Osterbrock (1989), we find for  $10000 \text{ K} \leq T \leq 20000 \text{ K}$ :

$$j_{\text{H}\alpha}/j_{\text{H}\beta} = 2.86 \left(\frac{T}{10^4 \text{ K}}\right)^{-0.057} \quad (\text{A11})$$

$$j_{H\beta}/j_{Pa\alpha} = 2.959 \left( \frac{T}{10^4 K} \right)^{0.251} \quad (\text{A12})$$

$$j_{H\beta}/j_{Br\gamma} = 35.939 \left( \frac{T}{10^4 K} \right)^{0.2454} \quad (\text{A13})$$

$$j_{H\beta}/j_{Br\alpha} = 12.496 \left( \frac{T}{10^4 K} \right)^{0.352} \quad (\text{A14})$$

These expressions are valid for densities  $100 \text{ cm}^{-3} \leq n_e \leq 1000 \text{ cm}^{-3}$ .

## REFERENCES

- Allen, M. L. & Kronberg, P. P. 1998, *ApJ*, 502, 218
- Altenhoff, W., Mezger, P. G., Wendker, H., & Westerhout, G. 1960, *Veröff, Sternwarte, Bonn*, No. 59, 48
- Beck, R., Brandenburg, A., Moss, D., Shukurov, A., & Sokoloff, D. 1996, *ARA&A*, 34, 155
- Beck, S. C., Turner, J. L., & Kovo, O. 2000, *AJ*, 120, 244
- Beck, S. C., Turner, J. L., Langland-Shula, L. E., Meier, D. S., Crosthwaite, L. P., & Gorjian, V. 2002, *AJ*, 124, 2516
- Blain, A. W., Smail, I., Ivison, R. J., & Kneib, J.-P. 1999, *MNRAS*, 302, 632
- Caplan, J. & Deharveng, L. 1986, *A&A*, 155, 297
- Chevalier, R. A. & Fransson, C. 2001, *ApJ*, 558, L27
- Clark, J. S. et al. 2001, *A&A*, 376, 476
- Condon, J. J. 1992, *ARA&A*, 30, 575
- Condon, J. J., & Yin, Q. F. 1990, *ApJ*, 357, 97
- Dale, D. A., Helou, G., Neugebauer, G., Soifer, B. T., Frayer, D. T., & Condon, J. J. 2001, *AJ*, 122, 1736
- Deeg, H., Brinks, E., Duric, N., Klein, U., & Skillman, E. 1993, *ApJ*, 410, 626
- Guseva, N. G., Izotov, Y. I., & Thuan, T. X. 2000, *ApJ*, 531, 776
- Haarsma, D. B., Partridge, R. B., Windhorst, R. A., & Richards, E. A. 2000, *ApJ*, 544, 641

- Helou, G. & Bica, M. D. 1993, *ApJ*, 415, 93
- Hunt, L. K., Vanzi, L., & Thuan, T. X. 2001, *A&A*, 377, 66
- Izotov, Y. I., Lipovetsky, V. A., Chaffee, F. H., Foltz, C. B., Guseva, N. G., & Kniazev, A. Y. 1997, *ApJ*, 476, 698
- Izotov, Y. I., Chaffee, F. H., Foltz, C. B., Green, R. F., Guseva, N. G., & Thuan, T. X. 1999, *ApJ*, 527, 757
- Klein, U., Weiland, H., & Brinks, E. 1991, *A&A*, 246, 323
- Klein, U., Wielebinski, R., & Morsi, H. W. 1988, *A&A*, 190, 41
- Klein, U., Wielebinski, R., & Thuan, T. X. 1984, *A&A*, 141, 241
- Kobulnicky, H. A. & Johnson, K. E. 1999, *ApJ*, 527, 154
- Kronberg, P. P., Lesch, H., & Hopp, U. 1999, *ApJ*, 511, 56
- Lampton, M., Margon, B., & Bowyer, S. 1976, *ApJ*, 208, 177
- Lang, C.C., Goss, W.M., & Rodríguez, L.F. 2001, *ApJ*, 551, L143
- Leitherer, C. 1990, *ApJS*, 73, 1
- Leitherer, C., Chapman, J., & Koribalski, B. 1997, *ApJ*, 481, 898
- Leitherer, C., Schaerer, D., Goldader, J. D., et al. 1999, *ApJS*, 123, 3
- Lequeux, J. 1980, in “Star Formation”, 10th Advanced Course Swiss Society of Astronomy and Astrophysics, Saas-Fee, eds. Appenzeller, I., Lequeux, J., & Silk, J., Geneva Observatory: Switzerland
- Liu, Q. Z., van Paradijs, J., & van den Heuvel, E. P. J. 2000, *A&AS*, 147, 25
- Madau, P., Ferguson, H. C., Dickinson, M. E., Giavalisco, M., Steidel, C. C., & Fruchter, A. 1996, *MNRAS*, 283, 1388
- Markarian, B. E., Lipovetskii, V. A., & Stepanian, D. A. 1983, *Astrofizika*, 19, 29
- Martí, J., Mirabel, I. F., Rodríguez, L. F., & Smith, I. A. 2002, *A&A*, 386, 571
- Melnick, J., Heydari-Malayeri, M., & Leisy, P. 1992, *A&A*, 253, 16
- Mezger, P. G. & Henderson, A. P. 1967, *ApJ*, 147, 471

- Mirabel, I. F., & Rodríguez, L. F. 1998, *Nature*, 392, 673
- Mohan, N. R., Anantharamaiah, K. R., & Goss, W. M. 2001, *ApJ*, 557, 659
- Muxlow, T. W. B., Pedlar, A., Wilkinson, P. N., Axon, D. J., Sanders, E. M., & de Bruyn, A. G. 1994, *MNRAS*, 266, 455
- Nagata, T., Woodward, C.E., Shure, M., Kobayashi, N. 1995, *AJ*, 109, 1676
- Oster, L. 1961, *Rev. Mod. Phys.*, 33, 525
- Osterbrock, D. E. 1989, “Astrophysics of Gaseous Nebulae and Active Galactic Nuclei”, University Science Books: Mill Valley, California
- Panagia, N., & Felli, M. 1975, *Å*, 39, 1
- Papaderos, P., Izotov, Y. I., Fricke, K. J., Thuan, T. X., & Guseva, N. G. 1998, *A&A*, 338, 43
- Pacholczyk, A. G. 1970, *Series of Books in Astronomy and Astrophysics*, San Francisco: Freeman, 1970
- Plante, S. & Sauvage, M. 2002, *AJ*, 124, 1995
- Press, W. H., Teukolsky, S. A., Vetterling, W. T., & Flannery, B. P. 1992, Cambridge: University Press, —c1992, 2nd ed.
- Pustilnik, S. A., Brinks, E., Thuan, T. X., Lipovetsky, V. A., & Izotov, Y. I. 2001, *AJ*, 121, 1413
- Rees, M. J. 1998, *Space Science Reviews*, 84, 43
- Rubin, R.H. 1968, *ApJ*, 154, 391
- Simon, M. 1969, *ApJ*, 156, 341
- Simon, M., Felli, M., Cassar, L., Fischer, J., & Massi, M. 1983, *ApJ*, 266, 623
- Smith, H. E., Lonsdale, C. J., Lonsdale, C. J., & Diamond, P. J. 1998, *ApJ*, 493, L17
- Tammann, G. A. 1982, *NATO ASIC Proc. 90: Supernovae: A Survey of Current Research*, 371
- Thuan, T. X., Bauer, F. E., Papaderos, P., & Izotov, Y. I. 2003, submitted

- Thuan, T. X., & Izotov, Y. I. 1997, ApJ, 489, 623
- Thuan, T. X., Izotov, Y. I., & Lipovetsky, V. A. 1997, ApJ, 477, 661
- Thuan, T. X., Sauvage, M., & Madden, S. 1999, ApJ, 516, 783
- Ulvestad, J. S. 1982, ApJ, 259, 96
- Vanzi, L., Hunt, L. K., Thuan, T. X., & Izotov, Y. I. 2000, A&A, 363, 493
- Verschuur, G. L. & Kellermann, K. I. 1988, Berlin: Springer, 1988, 2nd ed., edited by  
Verschuur, Gerrit L.; Kellermann, Kenneth I.,
- Weiler, K. W., Panagia, N., Montes, M. J., & Sramek, R. A. 2002, ARA&A, 40, 387
- Woltjer, L. 1972, ARA&A, 10, 129

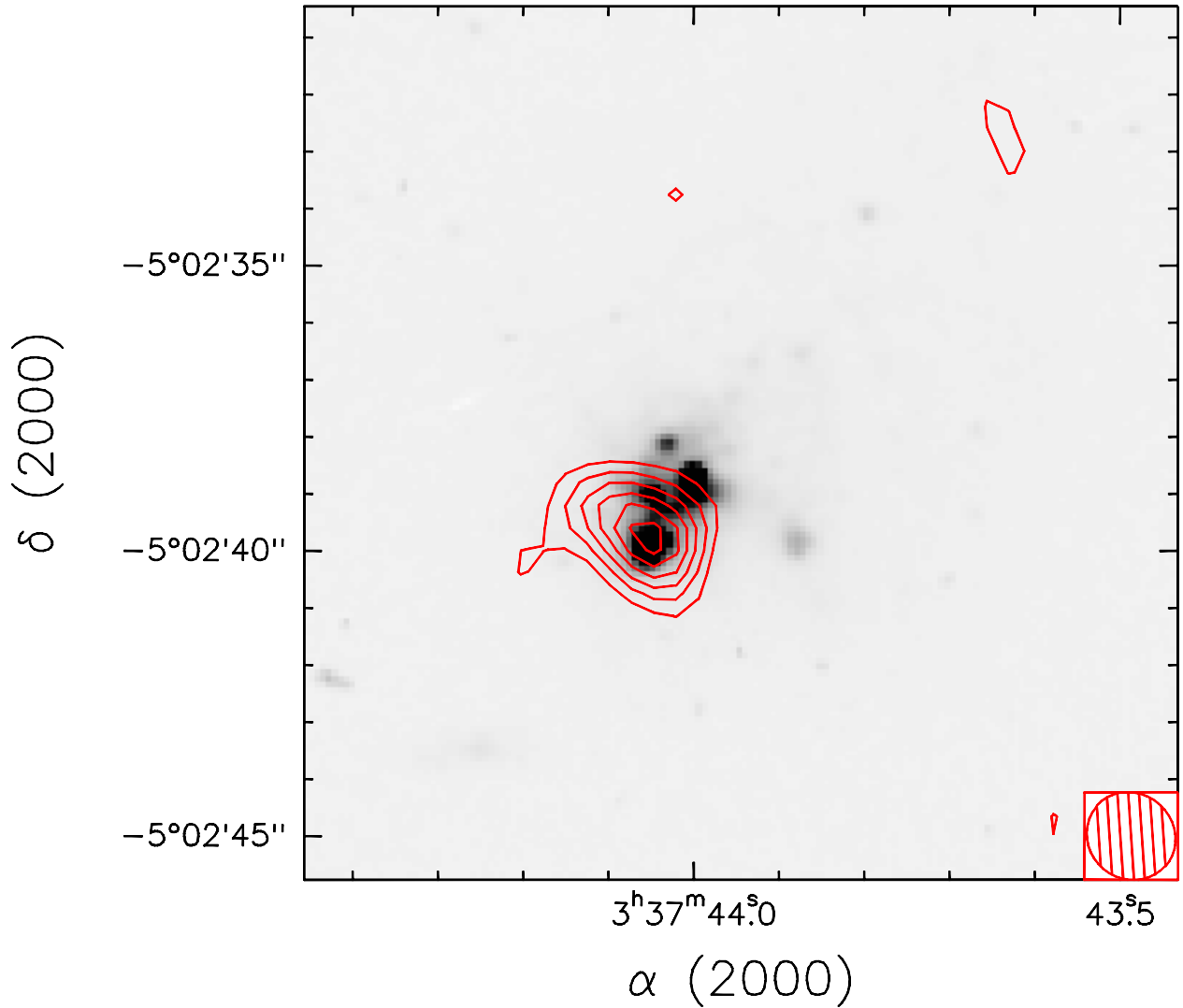


Fig. 1.— 20 cm map overlaid on the HST/WFPC2 (F791W) image. Radio contours run from 0.12 mJy/beam ( $2\sigma$ ) to 0.42 mJy/beam in units of  $\sigma$  (0.06 mJy/beam). The beam,  $1.6'' \times 1.5''$ , is shown in the lower right corner. The radio source is clearly coincident with the two brightest SSCs in the southeast portion of SBS 0335–052.



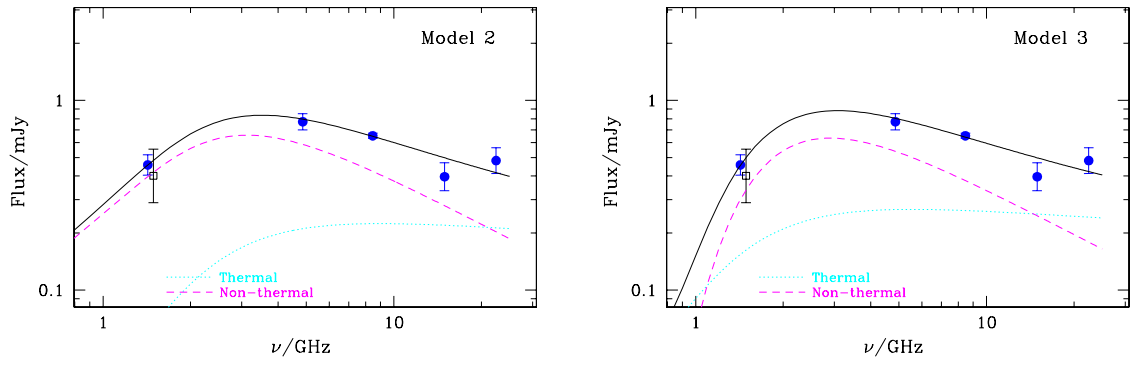


Fig. 2.— Radio continuum flux versus frequency  $\nu$ . Model 2 (mixed-geometry absorption of thermal+non-thermal components) is shown in the left panel, and model 3 (mixed-geometry absorption of thermal component + screen absorption of non-thermal one) in the right. The 1.49 GHz point denoted by a filled square is from Dale et al. (2001). A solid line shows the best-fit model, with the separate components given by a dotted line (thermal) and a dashed one (non-thermal).